Mon. Not. R. Astron. Soc. **302,** 139–144 (1999)

# The immersed echelle – I. Basic properties

R. Szumski and D. D. Walker
*Optical Science Laboratory, University College London, London WC1E 6BT*

Accepted 1998 September 1. Received 1998 August 18; in original form 1997 July 28

**ABSTRACT**

High-resolution spectrographs for very large telescopes lead to new challenges in grating technology to achieve optimum matching of the slit width to the seeing disc. This has led elsewhere to the development of long echelles of high blaze angle produced by mosaicking technology. An alternative approach, pursued in this paper and adopted for the Gemini High-Resolution Optical Spectrograph, is to immerse a monolithic echelle in a medium of refractive index greater than unity. This paper explores the consequences of this. It will be followed by Paper II, which will report on a major technology development programme in progress.

**Key words:** instrumentation: spectrographs – techniques: spectroscopic.

## 1 INTRODUCTION

Consideration of the immersed echelle as a possible enhancement of the standard echelle stems from the need to optimize the resolving power slit-width product of astronomical spectrographs for very large telescopes. The enhanced performance resulting from the immersion of a grating in a high-index ($n > 1$) dielectric medium has been described by Longhurst (1973), and more recently in greater detail by Dekker (1987) and Wynne (1991).

A research and development programme being undertaken by the Optical Science Laboratory (OSL) at University College London (Walker, Radley & Diego 1993) is currently addressing the performance benefits and design trade-offs that the immersed echelle presents. This is being driven by the scientific requirements for the Gemini High-Resolution Optical Spectrograph (HROS) that it should provide the maximum throughput, particularly in the UV, combined with the practical requirement of a compact instrument that will fit within the space constraints of the Gemini Cassegrain environment. Whilst the immediate context is Gemini, the methodology developed clearly has wider relevance. The underlying basis for this work is presented here, with the goal of general applicability to existing and new echelle spectrographs.

The principal difference between the immersed and non-immersed echelles is the presence of the enclosing high-refractive-index medium in the form of a prism. When light of wavelength $\lambda$ enters the prism, the effective wavlength of the radiation that the grating 'sees', $\lambda_e$, is actually smaller by a factor of $n$, the refractive index of the prism, i.e. $\lambda_e = \lambda/n$. Therefore, the ratio $\lambda_e/\sigma$ (where $\sigma$ is the grating constant or groove spacing) also decreases. It is this ratio that primarily determines the overall photometric efficiency of the echelle/prism combination. In addition, we may also interpret this to mean that the effective grating constant of the echelle has been increased by the factor $n$, and since the number of rulings remains unchanged, then this also leads to the result that the effective length of the echelle has increased by $n$.

Consequently, if the grating constant has increased, then the order of interference will also increase by $n$, resulting in a similar increase of resolving power $\mathcal{R}$. Thus intuitively it appears that the immersed echelle operates identically to an echelle, the effective grating constant and length of which have been multiplied by the immersing refractive index. The following sections explore the consequences of immersion in a more quantitative manner.

## 2 INTERFERENCE CHARACTERISTICS

The idealized operation of an immersed echelle is shown in Fig. 1. The entrance/exit face of the prism, F, is parallel to the facets of the echelle or grating, which is itself optically coupled to the prism, either by a suitable cement or oil. In this mode the acute angle denoted by $\theta_B$ is equal to the blaze angle. For the purpose of determining the angular position of outgoing rays the blaze angle is not required, as its sole purpose is to modify the diffracted energy distribution. This will be the subject of the next section.

Note that when the input and output beams are symmetrically disposed about the normal to the face F, then residual dispersions at the air/glass interface are cancelled. This is not the case when an asymmetry exists, but in real spectrographs this effect will be very small when compared with the much greater dispersion of the echelle.

### 2.1 The diffraction equation

Fig. 2 shows a grating immersed in a medium of refractive index $n$. A ray of wavelength $\lambda$ in air ($\lambda/n$ in the medium) is incident upon the rulings at an incidence angle of $\alpha$ with respect to the grating normal, or $\theta$ with respect to the grating facet normal, i.e. $\alpha = \theta_B + \theta$. The ray is then diffracted at an angle of $\beta$, or $\theta_B - \theta$ at the blaze peak. Constructive interference with an adjacent ray occurs when the following condition is satisfied:

$$m_n\lambda = n\sigma\cos\gamma(\sin\beta + \sin\alpha), \qquad m_n = \pm1, \pm2, \ldots, \text{etc.}, \quad (1)$$

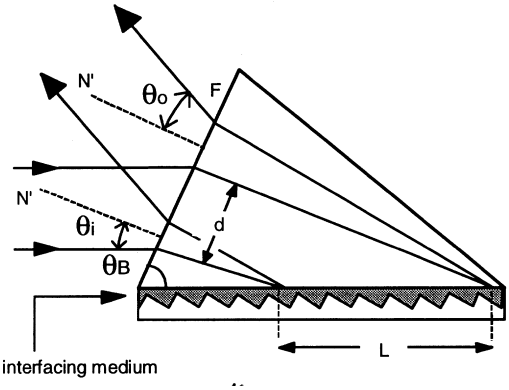


**Figure 1.** Operating configuration of immersed echelle in in-plane mode. N′ is the normal to F and the echelle facet.

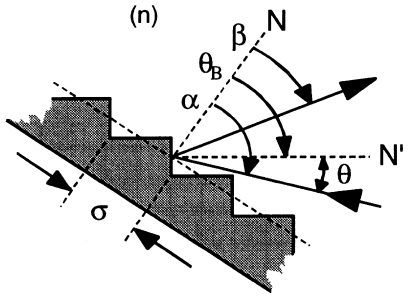


**Figure 2.** Local coordinate system for a ray incident on a facet of an echelle immersed in a medium of refractive index $n$. N is the normal to the echelle and N′ is the normal to the facet.

where $m_n$ is the *order of interference* when the echelle is immersed in a refractive index $n$, $\gamma$ is the *off-plane* angle between the ray and the plane of normal dispersion within the prism, and $\sigma$ is the ruling separation. In the *in-plane* condition (also commonly referred to as the Ebert Mounting), where the input and output rays and the facet normal are coplanar, the following is true when diffraction occurs at the *blaze-peak*:

$$\bar{m}_n\lambda = 2n\sigma \sin\theta_B \cos\theta, \tag{2}$$

where $\bar{m}_n$ is the order of interference at the blaze peak for wavelength $\lambda$, and $\theta \simeq \theta_i/n$ for small $\theta$. It is evident from the above that $\bar{m}_n$ is increased by a factor of the refractive index of the immersing medium, $n$, i.e. $m_n \simeq nm_{air}$, where $m_{air}$ is the order of interference if the echelle were immersed in air.

### 2.2 Free spectral range and dispersion

Diffraction gratings exhibit overlapping orders when two different wavelengths from adjacent orders are diffracted at the same angle. Thus, if two wavelengths $\lambda$ and $\lambda + \Delta\lambda$, originating from successive orders $m_n + 1$ and $m_n$, are similarly diffracted, then

$$(m_n + 1)\lambda = m_n(\lambda + \Delta\lambda), \tag{3}$$

which leads to

$$\Delta\lambda_{fsr} = \lambda/m_n, \tag{4}$$

where $\Delta\lambda_{fsr}$ is the *free spectral range*. The effect of immersing the grating in a high-index medium is to reduce the free spectral range in wavelength units by the factor $n$. The angular dispersion within the immersing medium is independent of the refractive index of the medium, as shown in equation (5):

$$\frac{d\beta}{d\lambda} = \frac{2\sin\theta_B \cos\theta}{\lambda\cos(\theta_B - \theta)}. \tag{5}$$

Upon leaving the prism the angular dispersion in air will increase by $n$, i.e.

$$\frac{d\beta'}{d\lambda} = \frac{2n\sin\theta_B \cos\theta}{\lambda\cos(\theta_B - \theta)} \qquad \text{for small } \theta, \tag{6}$$

where $\beta'$ is the angle of the diffracted ray in the air space in front of the prism.

The angular extent of the free spectral range $\Delta\beta_{fsr}$ within the prism is determined by integrating equation (5) with respect to $\lambda$ over the free spectral range to obtain

$$\Delta\beta_{fsr} = \Delta\lambda_{fsr}\frac{d\beta}{d\lambda} \qquad \text{where } \lambda \gg \Delta\lambda_{fsr} \tag{7}$$

$$= \frac{\lambda}{n\sigma\cos\gamma\cos(\theta_B - \theta)}. \tag{8}$$

For the diffracted beam in air, if it is assumed that $\Delta\beta_{fsr}$ is small and the beam leaves the prism at an angle near-normal to the exit face, then the total diffraction angle in air is given by

$$\Delta\beta'_{fsr} = \frac{\lambda}{\sigma\cos\gamma\cos(\theta_B - \theta)}, \tag{9}$$

where equation (9) shows that the angular subtense of the free spectral range is independent of $n$.

### 2.3 Resolving powers and spectrum matching

With most astronomical spectrographs, the resolving power is usually the starting point for the evolution of the design, since it relates directly to the astronomical case. In the majority of applications, including the baseline design for Gemini HROS, the resolving power is limited by the entrance slit and not the echelle ruling. However, an ultra-high-resolution capability for Gemini may be considered in the future, following the UCL Ultra-High-Resolution Facility at the AAT. This could in principle be an extension of HROS itself, or, more likely, a separate (eg fibre-fed and bench-mounted) instrument. Therefore, the ultimate resolving power of an echelle is of considerable interest.

In the diffraction-limited case,

$$\mathcal{R}_d = \frac{2nd_c\sin\theta_B}{\lambda}\left[\frac{\cos\theta}{\cos(\theta_B + \theta)}\right], \tag{10}$$

and for the Littrow mode,

$$\mathcal{R}_d = \frac{2nd_c\tan\theta_B}{\lambda}, \tag{11}$$

where $\mathcal{R}_d$ is the diffraction-limited resolving power and $d_c$ is the beam diameter prior to entering the prism.

The expression $2nd_c\tan\theta_B$ is actually the optical path difference along the beam diameter when in Littrow mode, as noted by Dekker (1987), and is referred to as the optical *depth* of the prism. Clearly, the effect of the immersing index is to provide a proportionate increase in the optical depth of the echelle, and with it the diffraction-limited resolving power. Note that the equivalent increase in resolving power could not necessarily be achieved by using a longer mosaicked echelle of higher blaze angle, unless the mosaic were precisely phased.

The slit width in arcsec projected on the sky can be related to the slit-limited resolving power $\mathcal{R}_s$ by standard equations governing the projection of solid angles through the entire optical system. A

useful formulation for designing an echelle spectrograph, which embodies the constraints of matching of the echellogram to the detector, is given by Walker & Diego (1985). When rewritten with the immersion index $n$, these equations become

$$\mathcal{R}_s = \frac{2n\sigma x \cos\theta \sin\theta_B \cos\gamma}{P\lambda_{max}}, \tag{12}$$

where $x$ is the detector width in the echelle dispersion direction, $P$ is the projected slit width (e.g. two pixels) and $\lambda_{max}$ is the nominal wavelength of the longest order for which the free spectral range will fit across the detector width $x$. The slit width $S$ in arcsec projected on the sky is given by

$$S = (2.06 \times 10^5) \times \frac{LP\lambda_{max}}{D_{tel}\sigma x \cos\gamma}, \tag{13}$$

where $L$ is the ruled length of the echelle, and $D_{tel}$ is the telescope aperture.

The required camera focal length $F_{cam}$ is

$$F_{cam} = \frac{\sigma x \cos\beta \cos\gamma}{\lambda_{max}}. \tag{14}$$

## 3 DIFFRACTION CHARACTERISTICS

In order to predict the relative energy distribution within the spectrum, it is necessary to combine the results above with information concerning the diffraction mechanism.

### 3.1 Single-slit diffraction

The blazed echelle grating may be viewed as a series of long slits, each acting as a source providing an output consistent with the incoming radiation in both wavelength and phase. The normalized angular intensity distribution across a slit of finite width is given by

$$I(\delta) = \left(\frac{\sin\delta}{\delta}\right)^2, \tag{15}$$

where $\delta$ is the phase difference between the centre and edge of the slit at the specified angle of diffraction, thus

$$\delta = \frac{2\pi}{\lambda} s \sin\left(\frac{\psi}{2}\right) \cos\left(\theta - \frac{\psi}{2}\right), \tag{16}$$

where $\psi = \beta - \bar{\beta}$ and $\bar{\beta}$ is the angle of diffraction corresponding to specular reflection at the slit facet, which is also identical to the blaze peak. The effective width of the diffracting aperture is $s$, where $s = \sigma\cos(\theta_B + \theta)/\cos\theta$, for $\alpha > \theta_B$. Since in this case the incident wavelength $\lambda_e$ is actually $\lambda/n$, an alternative description may regard equation (16) (and the corresponding angular intensity distribution) as being identical to that for an air-immersed echelle having a grating constant $n$ times larger than that of the immersed echelle. As expected, the total area beneath the curve given by equation (15) is an expression of the total energy incident upon the diffracting aperture.

### 3.2 Echelle efficiency

The distribution of energy within any particular order relative to the blaze peak is to a first approximation given by the same function as equation (15) (Schroeder 1980; Bottema 1981), except for a constant multiplying factor $\epsilon$, the diffraction efficiency:

$$I(\delta) = \epsilon\left(\frac{\sin\delta}{\delta}\right)^2, \tag{17}$$

while $\epsilon$ satisfies the following:

$$\sum_{\Delta m=-\infty}^{\infty} \epsilon\, I(\delta) = 1, \tag{18}$$

where $\Delta m = \bar{m}_n - m_n$ and $\delta$ is obtained by substituting the following into equation (16):

$$\sin\beta = \sin\bar{\beta} - 2\left(\frac{\Delta m}{\bar{m}_n}\right)\sin\theta_B\cos\theta. \tag{19}$$

Naturally, the only values of $m_n$ that need to be considered in the above summation are those that are physically realizable.

It should be noted that in deriving equations (17)–(19) no explicit attempt was made to obtain similar expressions for the air space preceding the prism. The reason for this is that the result is effectively the same. The relationship between the slit-facet far-field diffraction pattern and the grating interference pattern remains unchanged, regardless of which space it is viewed from. If the blaze function were plotted for the two spaces then differences would result from the varying angular extents of the free spectral ranges, but, as explained in the note below, when plotting is undertaken in terms of the free spectral range as a unit then the two curves will be identical. Even this statement is not completely true, as the transformation from angular coordinates in the prism to the surrounding air space would not be wholly linear.[1]

The underlying mechanism that determines the grating efficiency depends upon the manner in which the single-slit diffraction pattern and the various grating orders overlay one another. If the positions of several grating orders, at a specific wavelength, correspond to local subsidiary maxima of the slit function then energy is considered to *leak* into these side orders at the expense of energy that could be more usefully employed in the blaze-peak order. This *leaking* process results in a lowering of the intensity level at the blaze peak.

Ideally, all orders, except for the blaze-peak order which is located at the central maximum, would be required to be positioned at the local minima of the slit function. In general, this is not practically realizable. On the other hand, from a theoretical point of view, if a glass could have a sufficiently high refractive index then it might indeed be so. The three blaze functions presented in Fig. 3 are of an immersed echelle in Littrow mode ($\theta = 0, \gamma = 0$), where the immersing index is $n = 1$ (air), $n = 4$ (germanium, an IR transmitting material) and the hypothetical case of $n = 100$. The trend is clear but not over-pronounced: as $n \to \infty$ then $I_{pk} \to 1$, although half the improvement occurs in the step from $n = 1$ to $n = 4$.

For an explanation of this effect it is necessary to reconsider the manner in which the slit function and the diffraction orders overlay. Increasing the refractive index results in the free spectral range having a smaller angular extent within the prism, whilst the various diffracted orders are separated by similarly smaller angles. The angular position of the first slit-function minimum with respect to the central maximum, and the angular separation of the blaze-peak order, $\bar{m}_n$, and $\bar{m}_n \pm 1$ is approximately given by $\Delta\beta = \lambda/(n\sigma\cos\theta_B)$, for small $\Delta\beta$. As the angle decreases, by increasing $n$ or $\sigma$ or by decreasing $\lambda$, then the deviation from $\Delta\beta$ for other order separations, i.e. between $\bar{m}_n + 2$ and $\bar{m}_n + 3$, also

[1] Note that the blaze-function graphs that are discussed follow a convention that has been adopted at the Optical Science Laboratory for several years; in plotting the blaze function curve (or *blaze profile*), the units of the horizontal axis are in order numbers relative to $\bar{m}$ rather than the usual angular units. Thus the region between $\pm 0.5$ denotes the free spectral range. Such a coordinate transformation allows us to view the blaze function without the complications introduced by varying dispersions or free spectral ranges.

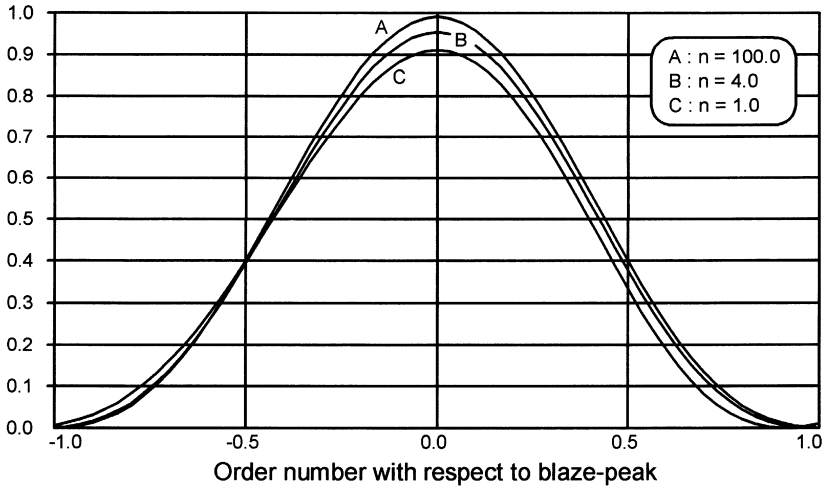


**Figure 3.** Blaze function curves for three immersing refractive indices. Conditions set are $\theta_i = 0°$, $\gamma = 0°$, $\lambda = 5000$ Å, $\sigma = 79$ g mm$^{-1}$, $\tan\theta_B = 2.0$.

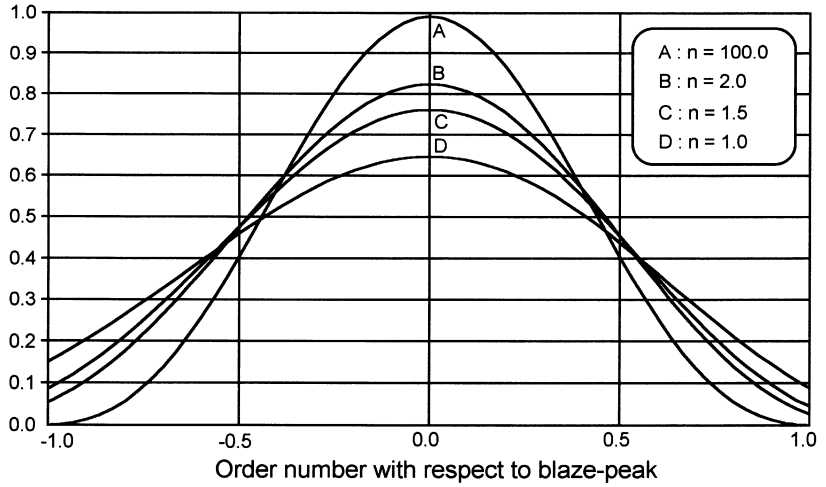


**Figure 4.** Blaze function curves for four immersing refractive indices. Conditions set are $\theta_i = 6°$, $\gamma = 0°$, $\lambda = 5000$ Å, $\sigma = 79$ g mm$^{-1}$, $\tan\theta_B = 2.0$.

decreases. This trend towards constant interorder angles has the benefit of positioning these same orders ever closer to the slit function minima. In such a circumstance, all the energy within a narrow wavelength band will lie in the blaze-peak order, and so $\epsilon \rightarrow 1$.

Consideration will now be given to the case where the immersed echelle is operated in the *in-plane* mode, that is $\theta_i > 0$ and $\gamma = 0$, where $\theta_i$ (see Fig. 1) is the incidence angle in the air space preceding the prism. Fig. 4 shows the variation in the blaze profile as the refractive index of the immersing prism increases from 1 to 2 in steps of 0.5, and a final step corresponding to $n = 100$. The trend clearly shows that the greatest change in the peak intensity ($I_{pk}$) occurs for small values of $n$, with $I_{pk} \rightarrow 1$ as $n \rightarrow \infty$.

The improvements in the blaze profile are almost entirely attributable to the diminishing value of $\theta$ within the prism as $n$ increases. This becomes evident when two gratings of $n = 1$ (air) and $n = 2$ are compared, where the incidence angle is $\theta_i = 3°$ for the former and 6° for the latter, i.e. $\theta = 3°$ *within* each prism. Though the blaze profiles are not presented, they are in fact almost identical, thus confirming the hypothesis.

The *off-plane* or quasi-Littrow mode ($\theta = 0$ and $\gamma > 0$) does not offer any benefit attributable to reduced $\theta$ at the echelle, as observed above, since $\theta$ is already zero. There is only a slight increase in efficiency as the echelle is immersed, because of improved matching of the slit function with the order pattern, resulting from decreasing wavelength at the echelle. If immersion in available glasses is considered, up to a maximum of $n = 4$ (germanium), then the improvement in $I_{pk}$ amounts to, at most, only 2–3 per cent. In other respects, performance parameters such as free spectral range and dispersion behave as expected.

## 4 APPLICATION OF THE THEORY

The anaysis above has described the operation of the immersed echelle in terms of quantities that bear directly on the free spectral range. Before attempting to undertake a simple design task employing an immersed echelle, other performance parameters that describe the energy distribution within the free spectral range have to be defined. These parameters are briefly discussed below.

(i) Peak value, $I_{pk}$ – the maximum signal level at the centre of the free spectral range. This may be of particular importance if a small spectral region of interest can be positioned at this point.

(ii) Minimum value, $I_{min}$ – the average signal level at the two ends of the free spectral range. This parameter is required when it is

necessary to ensure a minimum signal level above some pre-defined threshold.

(iii) Modulation, $M$ – the degree to which the signal intensity across the free spectral range deviates from a constant value, defined as $(I_{pk} - I_{min})/(I_{pk} + I_{min})$, where $I_{min}$ is the average value at the two ends of the band. A low value of $M$ is desirable in order to minimize photometric corrections, whilst a high value is indicative of a comparatively high $I_{pk}$ with respect to $I_{min}$.

(iv) Average value, $I_{avg}$ – the average signal level across the free spectral range.

Because of symmetry, the above four parameters are not all required for a proper description of the blaze function; in fact, any two parameters will suffice.

### 4.1 A simple illustration

Consider an echelle operating in an in-plane configuration in air, where changes are required to improve the resolving power slit-width product, without substantially altering the camera optics or format of the resulting echellogram.

Optical and performance parameters of the standard echelle (1) and an echelle immersed in fused silica (2) are shown in Tables 1 and 2 (some of the numerical results are obtained from real ray-tracing and not from the preceding equations, which themselves are based upon approximations such as constancy of dispersion over a wavelength interval). Note that, whilst the free spectral range has been reduced to $1/n$ of its former value, the angular subtense remains approximately the same. This is in agreement with equation (9). In addition, $I_{pk}$ has increased by a further 11 per cent while $I_{min}$ remains approximately unchanged.

**Table 1.** Echelle configuration variables.

| # | $\theta_i$ | $\tan\theta_B$ | $n$ | $1/\sigma$ |
|---|---|---|---|---|
| 1 | 6.0 | 2.00 | 1.00 | 79 |
| 2 | 6.0 | 2.00 | 1.46 | 79 |
| 3 | 6.0 | 2.00 | 1.46 | 117 |
| 4 | 6.0 | 2.00 | 1.46 | 75 |

Units: $\theta_i$ – degrees (°), $\sigma$ – mm.

**Table 2.** Echelle performance parameters at λ∼ 5000 Å.

| # | $I_{pk}$ | $I_{min}$ | $M$ | FSR | $\Delta\beta'_{fsr}$ | $\bar{m}_n$ |
|---|---|---|---|---|---|---|
| 1 | 0.65 | 0.45 | 0.18 | 111.2 | 4.22 | 45 |
| 2 | 0.76 | 0.47 | 0.24 | 75.7 | 4.44 | 66 |
| 3 | 0.77 | 0.47 | 0.24 | 110.0 | 6.54 | 45 |
| 4 | 0.75 | 0.46 | 0.24 | 71.0 | 4.20 | 70 |

Units: $\beta'$ – degrees (°), FSR – angstroms (Å).

The target system will ideally have a similar resolving power to echelle 2 whilst maintaining the free spectral range (FSR) and $\Delta\beta_{fsr}$ of echelle 1. Clearly, a better solution will require modifications to the configuration variables. Systems 3 and 4 have been identified as partial solutions that satisfy two of the three design targets. The first of these solutions is obtained by increasing the grating frequency to effect a change in the free spectral range, bringing it in line with echelle 1. In doing so, $\Delta\beta_{fsr}$ has increased by 50 per cent, but the blaze function profile has remained virtually unchanged. Echelle 4 takes a similar approach, but attempts to retrieve $\Delta\beta_{fsr}$ by reducing the grating frequency. The consequence of this is that FSR has been reduced by 56 per cent with, again, little change to the blaze profile. In both cases the resolving power remains unaffected, as this is primarily dependent on $\theta_B$. The blaze profiles for these echelles are shown in Fig. 5 for comparison.

The absence of a solution that meets all the target criteria is naturally the result of insufficient variables and excess parameters needing to be controlled. The only true variable is the groove frequency, which has been used to modify both $\Delta\beta_{fsr}$ and FSR, but not independently of one another.

## 5 GENERAL OBSERVATIONS

The previous analysis of the immersed echelle permits several general observations to be made concerning the various operational performance parameters. These are briefly discussed below.

(i) Dispersion – it has been shown that the dispersion within the immersing prism is, to a first approximation, independent of the immersing index ($n$), but is proportional to the immersing index when the light finally leaves the prism. Thus, an immersing prism of index 1.5 will provide a 50 per cent increase in dispersion compared with the same echelle in air.

(ii) Free Spectral Range (FSR) in wavelength units – this parameter is reduced by the factor of the immersing index. This result combined with the previous one leads to the next two conclusions.

(iii) Angular extent of the FSR – this remains virtually unchanged.

(iv) Number of orders – since the FSR is reduced by the factor $n$,

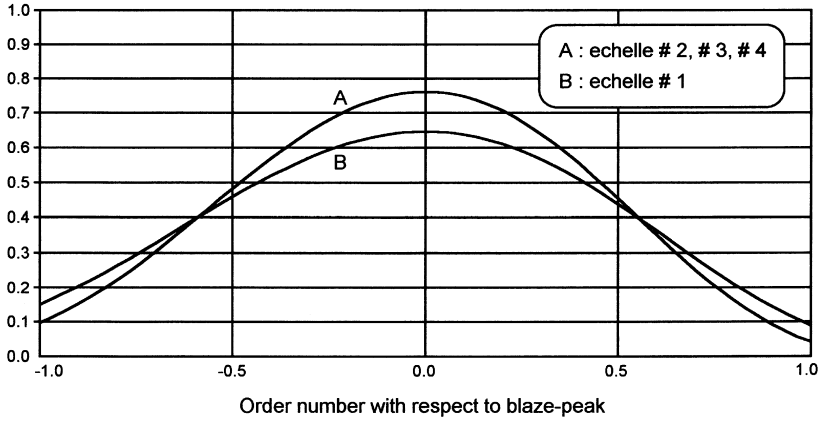


**Figure 5.** Blaze profiles – see text for explanation. Conditions set are $\theta_i = 6°$, $\gamma = 0°$, $\lambda = 5000$ Å.

then approximately $n$ times as many orders require to be captured to cover the same waveband.

(v) Order separation – whilst this is not a sole property of the echelle, for a given cross-disperser the order separations depend on the wavelength extents of the FSR, and so will be closer together by a factor $1/n$ on immersing the echelle.

(vi) Resolving power – as previously discussed, the diffraction-limited resolving power increases by a factor of $n$.

In addition, two other important observations may be made that lead to a simpler understanding of the efficiency benefits.

(vii) In general, reducing the wavelength of radiation incident upon an echelle in air results in small diffraction efficiency gains within the FSR. Identical benefits ensue when an echelle is immersed in a high-index medium, since the wavelength of the incident radiation is reduced to $1/n$ of its air-equivalent wavelength.

(viii) The Littrow configuration offers the highest efficiency gains, but is generally not employed. The reason for this is the difficulty (without additional elements such as those in 'white-light pupil' designs) of inserting camera optics that do not vignette the incoming beam. In practice, the incoming and outgoing beams are usually seperated by several degrees, which results in a reduction of peak diffraction efficiency. However, the efficiency depends on the beam separation *within the immersing medium*, rather than that in air. Since this angle is reduced by a factor of about $1/n$ in the medium, there is a significant efficiency gain on immersing an echelle, for a given camera-collimator geometry.

The case dealt with in the previous section illustrates available design options. In this particular illustration, we showed how to upgrade an existing echelle using one that has an improved resolving power slit-width product. By trading off the newly acquired increase in $\mathcal{R}_{\rm d}$ (obtained by immersing the echelle) against an increase in slit width, improvements are obtained in the overall throughput.

The two solutions presented will result in modifications to other subsystems of the spectrograph. For instance, the increased $\Delta\beta_{\rm fsr}$ of echelle 3 will lead to a corresponding decrease in the focal length of the camera optics, if the original detector format is to be retained. Similarly, the reduced FSR of echelle 4 will require a greater number of distinct orders to cover the operating waveband. If the slit length is to be maintained then this can only be achieved by increasing the cross-dispersion, possibly by combining a double-pass cross-dispersing prism with the immersing prism, as suggested by Walker et al. 1993. Other changes, such as anamorphic magnification, may be introduced to the system in order to facilitate the modified echelle, but it was not the intention of this paper to discuss such system-level implications in any detail.

Finally, the immersed echelle poses several practical problems in its implementation. Most difficult is the design of an adequate supporting structure for the possibly considerable weight of the prism, particularly at the Cassegrain focus. Also, the immersion prism presents a single air/glass interface that can reflect a ghost into the camera field. However, this can be eliminated by inclining the entrance face of the immersing prism, which can also conveniently provide some cross-dispersion. Similarly, the coupling medium between the immersing prism and the echelle must be free of absorption and scattering and provide a good index match to the prism. Finally, with some immersive materials, scattering could be a problem, leading to an increase in background signal. Fortunately, with laser-quality materials such as synthetic fused silica, this is not a problem even over long path-lengths. In cases where the immersing material does provide significant scattered light, it can be significantly reduced in a *post-echelle* disperser (where order seperation occurs after the echelle) by re-imaging the slit through a slit baffle, as suggested by Dekker (1987).

## 6 CONCLUSION

We have shown how the resolution × slit-width product is, on immersing an echelle, increased by a factor equal to the refractive index $n$ of the immersing medium. We have also demonstrated that there are theoretical gains in the intrinsic blaze efficiency as well. In the specific case of a diffraction-limited spectrograph, the limiting resolving power $\mathcal{R}_{\rm d}$ is also increased by the factor $n$.

The impact on the echellogram format of taking a traditional cross-dispersed echelle spectrograph and substituting the same echelle but immersed in a prism of index $n$ that is (i) the echellogram occupies the *same* footprint on the detector, (ii) each order has $n$ times the previous dispersion, (iii) each order contains $n$ times smaller wavelength extent, and consequently (iv) the cross-dispersed orders are $n$ times closer together. The increased dispersion is the origin of the increased resolution × slit-width product, and it is paid for in reduced order spacing.

Following the above results, the Gemini project has adopted an immersed echelle for HROS, and the practical aspects of its construction are now under development.

## ACKNOWLEDGMENTS

This work was enabled by EPSRC award 92597695 under the auspices of the Sira/UCL(CAIS) Postgraduate Training Partnership. The authors acknowledge comments from an independent referee.

## REFERENCES

Born M., Wolf E., 1965, Principles of Optics, 3rd edn. Pergamon Press, pp. 401–407
Bottema M., 1981, Appl. Opt., Vol. 20, No. 4, p. 528
Chaffee F. H., Jr, Schroeder D. J., 1976, ARA&A, 14, 23
Dekker H., 1987, in Robinson L. B., ed., Instrumentation for Ground-Based Optical Astronomy. Springer-Verlag, Berlin, p. 183
Engman S., Lindblom P., 1982, Appl. Opt., Vol. 21, No. 23, p. 4356–4362
Longhurst R. S., 1973, Geometrical and Physical Optics. Longman, London, p. 27
Schroeder D. J., Hilliard R. L., 1980, Appl. Opt., Vol. 19, No. 16, p. 2833–2841
Walker D. D., Diego F., 1985, MNRAS, 217, 355
Walker D. D., Radley A., Diego F., 1993, The High Resolution Optical Spectrograph for Gemini – A Design Study, Final Report, University College London, London
Wynne C. G., 1991, MNRAS 250, 796

This paper has been typeset from a TEX/LATEX file prepared by the author.